PAPER

Modelling intrinsic error field correction experiments in MAST

IOP Publishing Plasma Physics and Controlled Fusion

Plasma Phys. Control. Fusion **56** (2014) 104002 (17pp) doi:10.1088/0741-3335/56/10/104002

Modelling intrinsic error field correction experiments in MAST

Yueqiang Liu, A Kirk, A J Thornton and The MAST Team

Euratom/CCFE Fusion Association, Culham Science Centre, Abingdon, OX14 3DB, UK

E-mail: yueqiang.liu@ccfe.ac.uk

Received 23 December 2013, revised 12 March 2014
Accepted for publication 28 March 2014
Published 27 August 2014

Abstract

Optimal correction of the intrinsic, static error field (EF) by the correction coils in MAST is numerically studied, based on linear, full MHD plasma response computed in full toroidal geometry. Various optimization criteria are proposed, and the results are compared with empirical optima from representative EF correction (EFC) experiments. The two best criteria are thus identified, one aiming at minimization of the net toroidal resonant electromagnetic torque produced on the plasma column by the EF, the other corresponds to the full cancellation of the 2/1 resonant field harmonic at the $q = 2$ surface, including the plasma response. Neither the vacuum field based criterion nor the singular value decomposition (including plasma response) based criteria produce satisfactory predictions for the EFC in MAST.

Keywords: error field, correction coils, MAST

(Some figures may appear in colour only in the online journal)

1. Introduction

It has been established in several tokamak devices [1–6] that tiny, non-axisymmetric static error fields (EFs), of Gauss level compared to the Tesla level axisymmetric toroidal field, can play a significant role in limiting the operational space, in particular for Ohmic plasmas. These 3D EFs come from various sources in a tokamak device, and are often machine dependent. The most prominent problem, caused by low-n (n is the toroidal mode number) EF, is probably the mode locking, as a result of the non-linear interaction between the plasma flow and the resistive mode (the tearing mode) in the plasma. This non-linear interaction often involves a bifurcation process, resulting in threshold values for the EF magnitude at a fixed plasma density, or the lowest accessible plasma density at a fixed EF. Beyond the threshold a positive feedback mechanism occurs, that facilitates the penetration of the EF into the plasma, accompanied by the damping of the plasma flow. The resulting locked mode often leads to the plasma disruption. The EF induced mode locking is a most severe issue in L-mode plasmas. This is also the plasma regime that we shall carry out our study in this work.

On the other hand, we should keep in mind that the EF may be an important issue also for H-mode plasmas, despite a better screening effect by a normally faster plasma flow in this plasma regime. Indeed there are several factors that make the EF correction (EFC) potentially important even for H-mode plasmas. First of all, the plasma flow speed may not be sufficiently high in machines like ITER. Secondly, high beta plasmas often strongly amplify the external EF, due to the response of marginally stable ideal kink modes. Another fact, which applies to both L- and H-mode plasmas, is that the non-resonant harmonics of the EF are not shielded by the plasma, and can hence freely penetrate through. Moreover, due to the toroidal coupling between the resonant and the non-resonant harmonics, even the resonant parts can re-appear inside the rational surfaces although they are screened at the surfaces. The resulting global 3D magnetic field perturbations, even in the presence of a perfect shielding, still induce global torques such as the neoclassical toroidal viscous (NTV) torque, that can be potentially large enough to brake the plasma rotation. The EFC has been extensively investigated in H-mode plasmas in experiments, not only associated with the mode locking [6, 7], but also in the context of high beta driven magnetohydrodynamic (MHD) mode control [6, 8, 9]. Finally, we point out that the EFC concept also applies to the reversed field pinch configurations [11].

Although feedforward control of the static EF is the main topic of discussion here, it is worthwhile to mention a

recently developed concept of DEFC, which is based on the feedback control of the EF, and has been first successfully applied in the DIII-D tokamak for either high beta [8] or low beta [10] plasmas. This DEFC concept, which mainly targets the low frequency spectrum of the sensor signal, has been shown to be essential in combination with the resistive wall mode control. For experimental scenarios where the plasma condition varies—which is often the case—during the discharge, the plasma response to the vacuum EF also varies, and hence the dynamic correction may indeed be crucial. Although the (empirically based) feedforward DEFC should also be an option, it appears that the feedback based DEFC may be a more robust technique.

Despite extensive experimental efforts in understanding the EFC using additional magnetic coils, modelling work is so far limited, with results mainly by the IPEC code [12, 13]. This is probably because the EFC modelling critically involves the geometry. A full toroidal geometry is essential, in order to provide useful recommendations for the optimal correction of the EF in a given device. On the other hand, the physics understanding of the EF penetration and the mode locking is less geometry dependent, and the theory has been well developed [14, 15].

The key goal of the EFC modelling is to propose optimization strategies or criteria that can be used for predicting optimal EFC for experiments. In a working device, the optimization criteria may be less urgent, since the optimal correction currents, of the EF correction coils, can usually be experimentally determined via the so called polar map approach [3]. It may be attempting to think that the optimal correction of the EFs can be experimentally established in ITER, when ITER is in operation. On the other hand, the polar map approach requires deliberate disruption of the plasma (via the mode locking), which may not be affordable in ITER. Therefore, if we wish to predict the optimal EFC for ITER, we have to establish certain optimization criteria that are well validated against present experiments. These criteria can in principle rely on more engineering parameters, such as the overlap criterion proposed for ITER [12], or more physics based parameters, such as those considered in this work. Either way should be applicable as long as the theory model can use the optimization criteria to predict the optimal correction currents.

In this work, we propose and examine several EFC optimization criteria when applied to the MAST experiments. We consider both the linear resistive plasma response with toroidal flow, and an ideal, static plasma response similar to that of the IPEC code. Because of the often complicated nature of the EF, we propose an efficient model of representing an (arbitrary) EF, via the concept of the equivalent surface current (ESC). This concept is described in the next Section. Section 3 discusses the linear plasma response, showing both the model and examples of results when applied to a MAST plasma. Section 4 proposes various criteria for the EFC optimization, with the modelling results, applying these criteria, reported in section 5. Comparisons of the modelling predictions with MAST EFC experiments are also reported here. Section 6 draws conclusion and discussion.

2. ESC representation of EF

A key factor in modelling the EFC is to have a simple but accurate way of representing the intrinsic EF as measured in experiments. In this work, we adopt a procedure that allows us to represent the EF by an ESC. This approach, together with its advantages and limitations, is described below.

We start the discussion by noticing that the intrinsic 3D EF often has a complicated nature in tokamak devices. This is the case also for MAST, where the non-axisymmetric EF is often associated with the shifting, tilting, etc., of certain equilibrium poloidal field (PF) coils. Therefore, a direct modelling of the current sources that generate the EF is often not easy, and certainly machine-dependent. On the other hand, it is often possible to directly measure in experiments the poloidal distribution of the vacuum EF along a given surface $S_{\rm EF}$ outside the plasma. The measured vacuum EF of course depends on the operational configuration of the machine (e.g. the currents in the PF coils). But with a fixed configuration, in theory we can always assume that the vacuum EF can be measured and therefore is known, at the surface $S_{\rm EF}$. In practice, as an example, MAST uses two arrays of Hall probes at two poloidal locations, that provide 12 uniformly distributed sensor signals for B_R and 24 uniformly distributed B_Z data (in the cylindrical coordinate system) along the toroidal angle [19]. These probes provide very accurate toroidal resolution for the low-n components of the intrinsic EF. These field data are fitted into the ERGOS code, in order to produce equivalent 3D current sources in terms of the PF coils shifting, titling etc., parameters, by effectively solving a parametrized inverse problem.

The measured intrinsic EF in MAST often has two dominant toroidal components: $n = 1$ and $n = 2$. However, most of the EFC experiments have been carried out for the $n = 1$ correction. And hence systematic database is available only for the $n = 1$ correction. On the other hand, when the EFC problem is treated linearly, as is the case in this study, there is no coupling to the other toroidal components. In other words, the $n = 1$ and the $n = 2$ EFC can be separately investigated without affecting the final computational results. In this work, we consider only the $n = 1$ correction. Consequently, we only include the $n = 1$ component of the intrinsic EF from MAST in our further study.

If we assume that there is no other external current sources (such as wall eddy currents, resonant magnetic parturbation (RMP) coils, ferromagnetic inserts, etc.) enclosed by $S_{\rm EF}$, the vacuum field is uniquely defined in the volume enclosed by $S_{\rm EF}$, by specifying the normal component of the EF at $S_{\rm EF}$. This follows from the uniqueness (up to a constant) of the solution of the Laplace equation for the vacuum field scalar potential, with the Neumann boundary condition. Therefore, the problem of representing the vacuum EF in the whole plasma domain is reduced to the prescription of the normal component of the EF at a surface just outside the plasma boundary.

Next, for a given normal component of the EF at a surface $S_{\rm EF}$, it is always possible to find an ESC, at another surface $S_{\rm ESC}$ outside $S_{\rm EF}$, that produces the given normal field (see figure 1 for the geometry). In fact an inductance matrix can

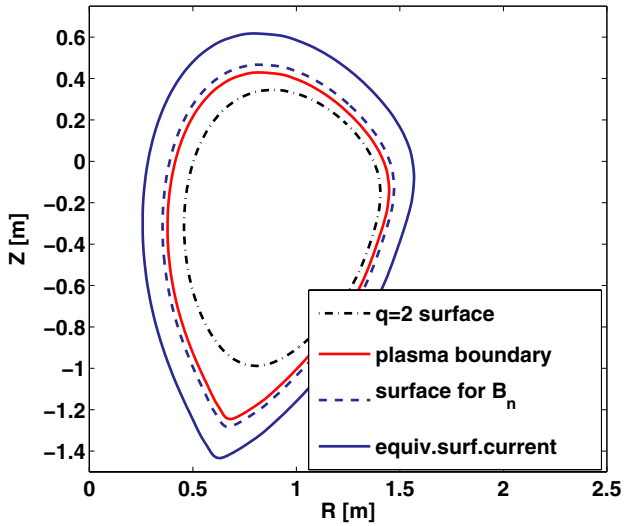

Figure 1. Geometry for representing the EFs by an ESC. The four surfaces are, from outside inwards, the surface S_{ESC} where the ESC is located, the surface S_{EF} where the total vacuum EFs (the normal component) are specified, the plasma boundary and the $q = 2$ surface.

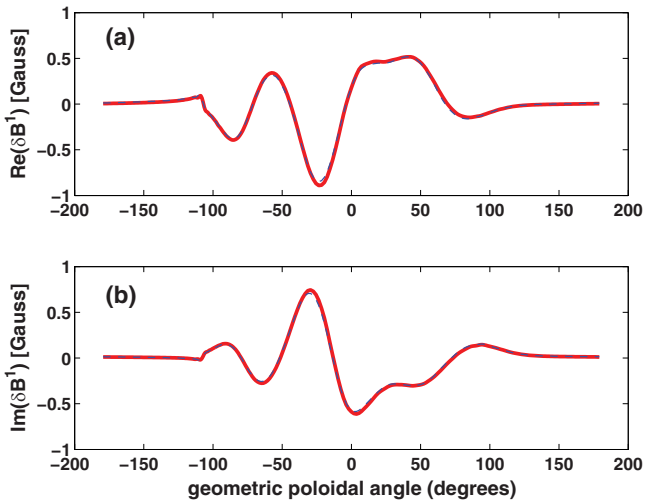

Figure 2. The (a) real, and (b) imaginary parts of $n = 1$ normal component of a test vacuum EF at the surface S_{EF}, plotted along the geometric poloidal angle θ. The outboard mid-plane is located near $\theta = 0$.

be calculated (appendix A), that relates the poloidal Fourier harmonics of the normal field at S_{EF}, to that of the ESC at S_{ESC}, in a generic toroidal geometry. Knowing the ESC, it is straightforward to compute the plasma response to the intrinsic EF.

The obvious advantage of this approach is the versatility—it does not depend on the exact sources that produce the intrinsic EF, as long as the normal field of the EF at one surface (just outside the plasma) can be measured or specified. The drawback is that the vacuum EF, and hence the plasma response field as well, is valid only inside the surface S_{EF} at which the normal component is assigned. This does not pose a limitation on the EFC study presented in this work, but may require further considerations if we wish to use the computed plasma response field, for instance, to model the energetic particle losses towards the plasma facing components which are beyond the surface S_{EF}.

We also mention that the ESC approach is only one of the possible ways of representing the boundary condition for the MHD equations. It is also possible to impose the boundary condition using the (external) field only. But in this case, both the normal and the tangential components of the vacuum field are required, and need to be combined in a proper way. One such example is shown in [16], where an eigenvalue problem is solved, and the ratio of the tangential to the normal field components serves as the proper boundary condition. For the plasma response computations, as carried out here, the ratio of the field components is not sufficient, since it lacks the information on the magnitude of the vacuum EF.

The above described ESC procedure has been implemented and tested in the MARS-F [17] code. An example is show below, based on an plasma equilibrium reconstructed from the MAST discharge 28002. Figure 1 shows various surfaces of interest—the $q = 2$ rational surface, the plasma boundary surface, the surface S_{EF} where the normal component of the vacuum intrinsic EF is specified, and the surface S_{ESC} where the ESC is computed.

In MAST experiments, the EF is measured, and a Biot–Savart law based current source model (involving the shifting, tilting, etc. of the PF coils) has been developed in the ERGOS code [18], that produces the equivalent EF as in experiments. [We refer to an accompanying paper [19] for details on the experimental aspects of the EF and EFC in MAST.] The normal component of the $n = 1$ vacuum EF for shot 28002 is plotted in figure 2, along the poloidal angle at the surface S_{EF}. This normal component is used as the input for MARS-F to construct the $n = 1$ ESC.

Figure 3 plots the MARS-F computed poloidal and toroidal components of the $n = 1$ ESC at the surface S_{ESC}. Note that this current density generally has a continuous distribution along the poloidal angle, and therefore cannot be represented simply by a finite set of coils.

One crucial test is whether the computed ESC as shown in figure 3 generates the same vacuum EF inside the plasma. (The ESC does accurately recover the input normal field component at S_{EF}. The recovered field is also plotted in figure 2, but cannot be distinguished from the input field.) Figure 4 compares the R- and Z-components (in cylindrical coordinates) of the $n = 1$ EF at the $q = 2$ surface inside the plasma, generated by the ESC and by the equivalent ERGOS model. The agreement is very good.

3. Linear plasma response

3.1. Toroidal response model

We use the MARS-F code to model the linear response of the plasma to the static, intrinsic 3D EF. MARS-F solves the single-fluid, perturbed MHD equations in full toroidal geometry. A generic formulation including the plasma resistivity and inertia, as well as a sheared toroidal flow

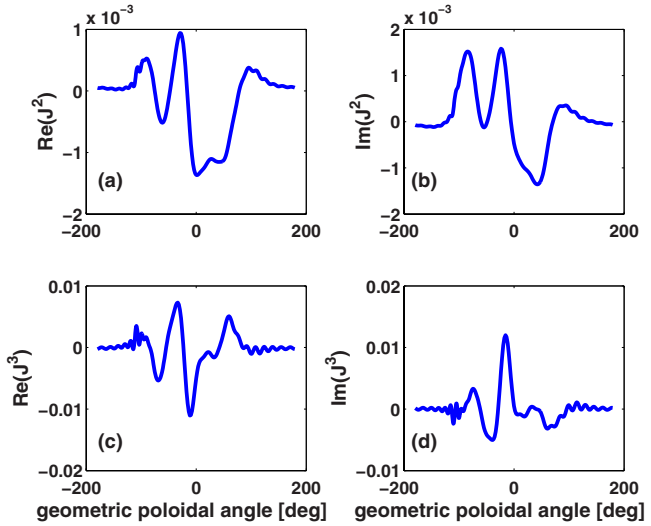

Figure 3. The computed poloidal (J^2) and toroidal (J^3) components of the $n = 1$ ESC at the surface S_{ESC}, plotted along the geometric poloidal angle.

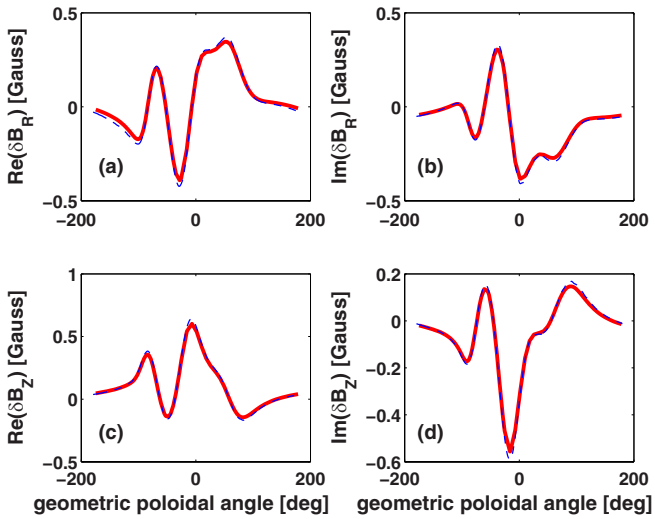

Figure 4. Comparison of the $n = 1$ vacuum δB_R and δB_Z fields computed at the $q = 2$ surface and generated by the ESC shown in figure 3, and the corresponding $n = 1$ vacuum EF at the $q = 2$ surface.

$\boldsymbol{V}_0 = R\Omega\hat{\phi}$, is envisaged

$$\mathrm{i}n\Omega\boldsymbol{\xi} = \boldsymbol{v} + (\boldsymbol{\xi}\cdot\nabla\Omega)R\hat{\phi}, \tag{1}$$

$$\begin{aligned}\mathrm{i}n\rho\Omega\boldsymbol{v} = &-\nabla p + \boldsymbol{j}\times\boldsymbol{B} + \boldsymbol{J}\times\boldsymbol{b}\\ &-\rho\left[2\Omega\hat{\boldsymbol{Z}}\times\boldsymbol{v} + (\boldsymbol{v}\cdot\nabla\Omega)R\hat{\phi}\right]\\ &-\rho\kappa|k_\parallel v_{\mathrm{th},i}|\,[\boldsymbol{v} + (\boldsymbol{\xi}\cdot\nabla)\boldsymbol{V}_0]_\parallel\,,\end{aligned} \tag{2}$$

$$\mathrm{i}n\Omega\boldsymbol{b} = \nabla\times(\boldsymbol{v}\times\boldsymbol{B}) + (\boldsymbol{b}\cdot\nabla\Omega)R\hat{\phi} - \nabla\times(\eta\boldsymbol{j}), \tag{3}$$

$$\mathrm{i}n\Omega p = -\boldsymbol{v}\cdot\nabla P - \Gamma P\nabla\cdot\boldsymbol{v}, \tag{4}$$

$$\boldsymbol{j} = \nabla\times\boldsymbol{b}, \tag{5}$$

where (R, ϕ, Z) represents the cylindrical coordinates. n is the toroidal harmonic number. The plasma resistivity is denoted by η. The variables $\boldsymbol{\xi}$, $\boldsymbol{v}$, $\boldsymbol{b}$, $\boldsymbol{j}$, p represent the plasma displacement, perturbed velocity, magnetic field, current, and pressure, respectively. The equilibrium plasma density, field, current, and pressure are denoted by ρ, $\boldsymbol{B}$, $\boldsymbol{J}$, P, respectively.

The above equations are written in a dimensionless form, with normalisation factors being R_0, B_0, B_0^2/μ_0, v_{A}, τ_{A}, for the length (displacement), the magnetic field, the pressure, the velocity, and the time, respectively, where B_0 is the toroidal vacuum magnetic field at the major radius R_0 of the magnetic axis, $\mu_0 = 4\pi\times10^{-7}\,\mathrm{H\,m^{-1}}$ is the free space permeability, $v_{\mathrm{A}} = B_0/\sqrt{\mu_0\rho_0}$ the on-axis toroidal Alfvén velocity, and $\tau_{\mathrm{A}} = R_0/v_{\mathrm{A}}$. The MHD equations are solved in a flux-based curve-linear coordinate system (see appendix A).

The last term in equation (2) describes the effect of parallel sound wave damping, where κ is a numerical coefficient determining the damping 'strength'. $k_\parallel = (n - m/q)/R$ is the parallel wave number, with m being the poloidal harmonic number and q being the safety factor. $v_{\mathrm{th,i}}$ is the thermal ion velocity. The parallel component of the perturbed velocity is taken along the equilibrium field line. Because $v_{\mathrm{th},i}$ is proportional to the square root of the equilibrium pressure, this damping term usually does not play a significant role for the response of low beta plasmas, which is the case for the MAST plasmas considered in this work. Nevertheless we have found that a large value of $\kappa \sim 1.5$ gives better results when compared with the MAST experiments.

In further discussions, we shall refer to the above plasma model as the resistive plasma response model.

Motivated by the recent successful EFC modelling based on an ideal, static plasma response (without flow) for DIII-D plasmas, using the IPEC code [13], we also compute the similar type of the plasma response by arranging the above MARS-F equations in a special way, namely we replace all the Doppler shift terms $\mathrm{i}n\Omega$ from the left hand side (LHS) of equations (1), (3) and (4) by the coefficient 1, remove the Doppler shift term from the LHS of equation (2), and remove all the terms from the right hand side associated with the toroidal flow, the plasma resistivity and the parallel sound wave damping term. The resulting equations are mathematically equivalent to the perturbed 3D equilibrium of an ideal plasma as used in the IPEC model. However, in the presence of rational surfaces inside the plasma, the above reduced ideal MHD equations form a global linear operator which is singular, and hence cannot be directly inverted in order to compute the plasma response. [The IPEC code employs an adaptive shooting method to avoid the problem of direct inversion of the global singular operator.] In order to resolve the singularity in the MARS-F approach, we add a small inertial term $\mathrm{i}\hat{\rho}\boldsymbol{v}$ to the LHS of equation (2), with $\hat{\rho}$ being small, of the order of 10^{-5}. In further discussions, we shall refer to this alternative, IPEC-like plasma model as the ideal plasma response model.

For the EFC modelling, we solve either the resistive or ideal plasma equations as defined above, together with the vacuum equation outside the plasma, and the ESC as a source term. The solution of the linear, antenna problem presents the steady state response of the plasma to the imposed intrinsic EF. This is similar to the RMP response computations that we have previously performed (and benchmarked) using the MARS-F code [20]. For the $n = 1$ plasma response computations in an equal-arc poloidal angle based coordinate system for MAST, we typically include 60 poloidal harmonics for the perturbed quantities.

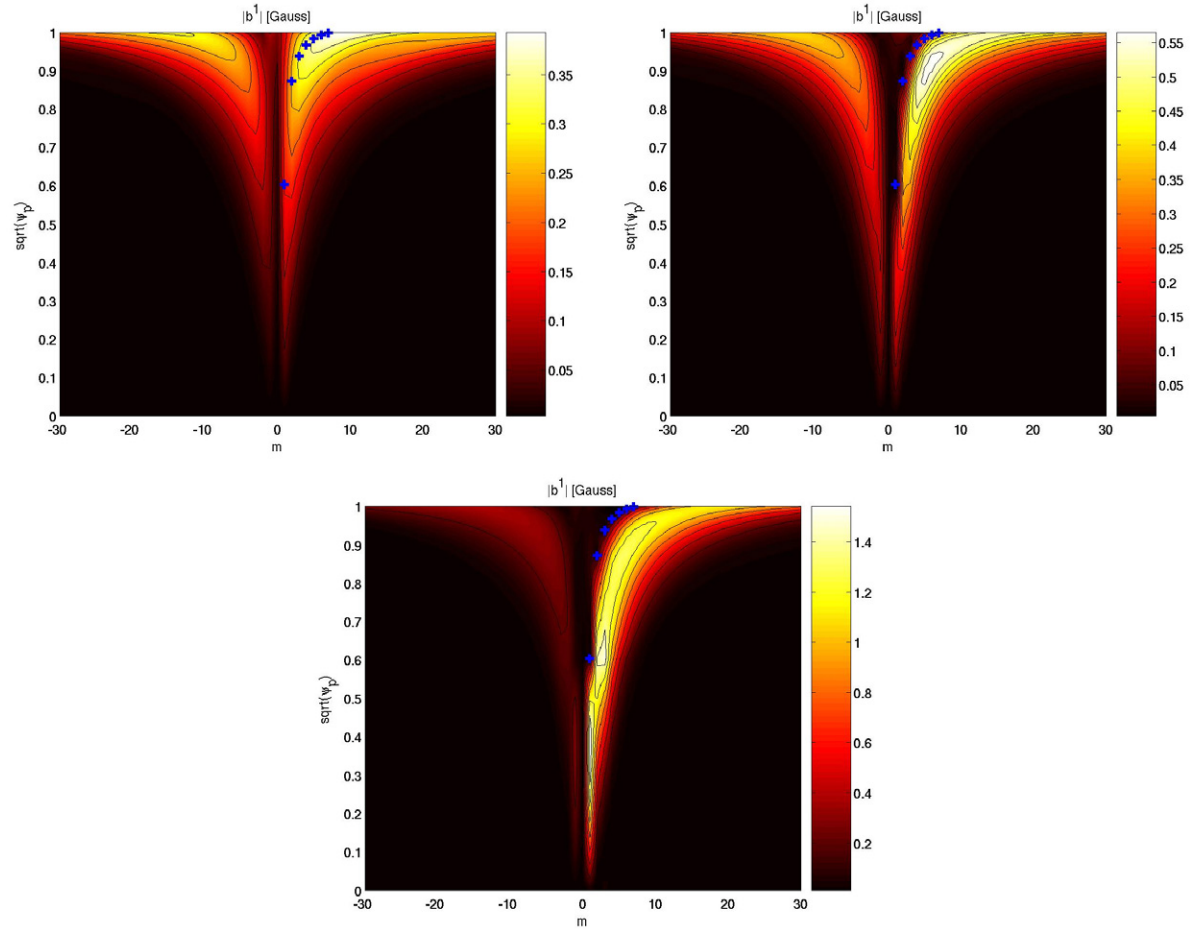

Figure 5. Computed poloidal spectrum (amplitude) of the normal field for (*a*) the vacuum EF only, (*b*) the total field including response from a resistive plasma, with toroidal flow, to the EF, and (*c*) the total field including response from an ideal plasma without flow. The symbols '+' indicate the location of rational surfaces. A MAST plasma from shot 26128 is used.

3.2. Computed plasma response

As an example, figure 5 compares the MARS-F computed poloidal spectrum (amplitude) of the normal component of $n = 1$ field for (*a*) the vacuum EF, (*b*) the resistive plasma response and (*c*) the ideal plasma response. The horizontal axis is the poloidal harmonic number m, the vertical axis is the plasma minor radius. The symbols '+' indicate the location of the corresponding rational surfaces ($q = 2, 3, 4, 5, 6, 7$ in this case). Both resistive and ideal response results in a significant reduction of the resonant field components near rational surfaces. This is expected for the ideal response, in which the resonant radial field vanishes at rational surfaces. For the resistive response, the reduction is most significant in the plasma core region, near the $q = 2$ rational surface. The reduction of the response of resonant field harmonics, at the corresponding rational surfaces, is the result of the plasma screening, which occurs within either the single fluid or two-fluid approximations. Even though the screening physics are somewhat different between these two models (appendix B), the eventual screening effect is similar. This gives one justification of adopting the single fluid model in the present EFC study, although the two fluid approach, such as that used in the M3D-C1 code [21], may represent a better screening physics. Nevertheless, as long as the plasma pressure is far below the no-wall beta limit for the ideal kink mode, it appears that the single fluid model gives reasonable predictions of the plasma response, compared to experiments [22].

We also note an amplification effect of the non-resonant components of the EF field, by both the resistive and ideal plasma response. The resistive model predicts an about 40% increase of the field amplitude, whilst the ideal model yields a much stronger amplification for this MAST plasma, by a factor of about 3. This is shown by the scale in the colour bar for each figure respectively. This amplification seems to be typical for MAST plasmas. Similar observations were made previously [23]. Most likely the response of a (marginally) stable ideal kink or peeling mode is responsible for this amplification effect [22, 24, 25]. For the purpose of the EFC, the amplification may affect the eventual results, to varying degrees, depending on the correction criteria that we choose.

4. Criteria for EFC optimization

In MAST experiments, two pairs of the external EFC coils (EFCC) are used to correct the $n = 1$ EF. Each pair produces the $n = 1$ field with currents flowing in the opposite direction in the two coils separated by 180° toroidally. The coils located at the 2nd and 8th sectors produce the current denoted as I_1

here. Similarly, the coils located at the 5th and 11th sectors produce the current I_2. This coil configuration produces very small, in fact in theory vanishing, $n = 2$ correction fields due to the toroidal symmetry of the coils.

The empirically optimal correction is found by performing locked mode experiments, where one pair of the coil currents are fixed, while scanning the currents in another pair, until the marginal correction point is found between the locking/unlocking, i.e. the locking current threshold. For a given plasma and a given EF configuration, this procedure normally yields four marginal correction points in terms of (I_1, I_2) (the so called polar map [3]). These four points often form a circle, the centre of which is defined as the optimal correction point. More details of the EFC experiments can be found in [19]. As will be shown in the next section, if the mode locking/unlocking is completely determined by a local linear quantity associated with, e.g. the corrected magnetic field perturbation or the plasma displacement, the four locking current threshold points should form a perfect circle.

The mode locking process obviously involves nonlinear physics [14, 15], for instance, the nonlinear interaction between the EF penetration and the damping of the plasma rotation. On the other hand, the EFC often aims at an optimal correction of the EF (according to certain criterion), such that the onset of the locking process does not occur. The simplest approach is to try to best correct the EF with EFCC, using the vacuum field as the approximation. The next possibility is to take into account the linear plasma response, and try to correct the total field. In this work, we consider both approaches, and compare the predicted optimal correction with the empirical data (in terms of the pair of the EFCC currents (I_1, I_2)). For this we first need to define and choose the optimization criteria. The criterion that gives the best match between the computed and the empirical optima can then be adopted for predicting the EFC in future experiments.

We adopt a systematic approach, by defining, *a priori*, a set of criteria, based either on certain components of the magnetic field (criteria A and D), or on the 3D plasma surface displacement (criteria C) as a result of the plasma response to the combination of the EF and the EFCC field, or on the net electromagnetic (EM) torque (criterion B). Details follow.

4.1. Criterion A: full cancellation of the 2/1 resonant field

According to this criterion, we choose the EFCC currents such that the $m/n = 2/1$ resonant component of the total field (EF + EFCC) vanishes at the $q = 2$ surface. The motivation of this choice is that the mode locking observed in experiments is often associated with the 2/1 tearing mode. For a strongly shaped plasma, the 2/1 Fourier harmonic is computed in a straight field line flux coordinate system.

Two possibilities are considered here: either the full cancellation of the vacuum field only, or that of the full field including the linear resistive plasma response. The ideal plasma response model (as defined in the previous section) is not applicable to this criterion, since the resonant harmonic always vanishes at the rational surface, with or without the correction of the EF.

4.2. Criterion B: minimization of the net EM torque

Since the mode locking is normally associated with the toroidal rotation braking of the plasma, it is natural to consider a criterion based on the toroidal momentum sink terms, i.e. the torques. There can be several physics mechanisms associated with the plasma response to the EF that lead to the momentum damping, including the resonant $\boldsymbol{j} \times \boldsymbol{b}$ EM torque, the NTV [26, 27], the Reynolds force $\rho(\boldsymbol{v} \cdot \nabla)\boldsymbol{v}$ associated with the plasma inertia and perturbed velocity, and field line stochastization (if this does occur during the EF penetration) induced momentum sink [28].

The present version of the MARS-F code computes the first three torques mentioned above, based on the computed linear plasma response. For typical MAST plasmas, the EM torque is larger than the NTV torque [23]. This is related to the fact that the plasma toroidal flow is normally fast in spherical tokamaks such as MAST, compared to typical toroidal flow speed in conventional aspect ratio tokamaks. For the modelled plasmas in this study, the toroidal rotation frequency of the core plasma can reach up to $150\,\mathrm{krad\,s^{-1}}$ (about 10% of the on-axis Alfvév frequency). The Reynolds torque is usually very small. For example, for the MAST plasma 28002 mentioned in section 2, the ratio between the computed net torques (across the plasma volume) are EM : NTV : Reynolds $= 1 : 0.39 : 0.003$, for the intrinsic EF induced torques, and EM : NTV : Reynolds $= 1 : 0.35 : 0.001$ for the EFCC induced torques with $I_1 = I_2 = -1\,\mathrm{kAt}$. This motivates our choice of the EM torque alone as one of the EFC criteria for MAST plasmas. We point out that, for other tokamak devices such DIII-D or JET, the NTV torque may be larger than the EM torque. Therefore, for those plasmas, it may be worthwhile to include the NTV torque as well in designing this type of the EFC criterion.

A typical MAST plasma has several rational surfaces even for the $n = 1$ response (q_{95} can exceed 7). We use the net EM torque across all the rational surfaces as the criterion for the EFC. An alternative choice is the torque associated with the 2/1 surface only. However, this leaves certain ambiguity in defining the torque, due to the fact that, for a realistic toroidal plasma, the computed EM torque density is often spread across a wide region near the resistive layer, and this spreading is often enhanced by the resonance effects with the continuum waves [29]. One example of the computed torque distribution is shown in figure 6.

We point out though, that in the case of a single rational surface, criterion B is somewhat directly related to criterion A (with the plasma response). This is because the optimal EFC following criterion A results in a vanishing resonant b_r field at the rational surface. On the other hand, the toroidal EM torque is mainly contributed to by the product of $j_\theta b_\mathrm{r}$, which should also vanish at the rational surface. However, there are at least two factors that decouple the Criterion B from A. One is the usually small, but yet finite contribution of the $j_\mathrm{r} b_\theta$ term to the toroidal torque, from a resistive plasma response. The other is the resonant splitting effect discussed in [29], resulting in a finite EM torque density away from the rational surface (where b_r vanishes following criterion A).

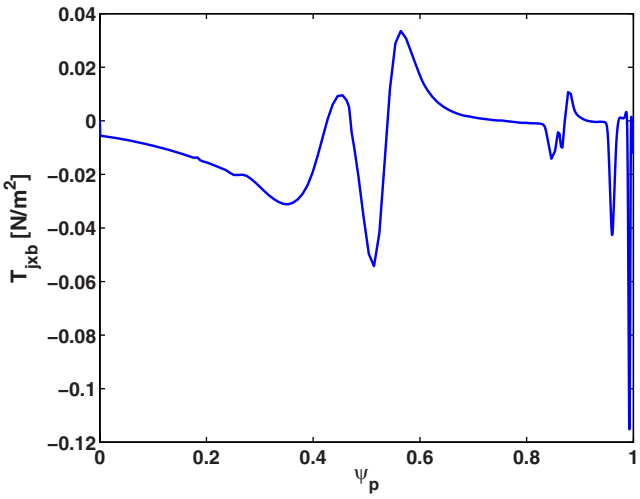

Figure 6. The computed fluid $j \times b$ toroidal EM torque density, induced by the intrinsic EF from the MAST discharge 28002.

4.3. Criterion C: minimization of plasma surface distortion

The non-axisymmetric external fields (e.g. EF and/or EFCC) cause 3D distortion of the plasma boundary. Consideration of an EFC criterion associated with the plasma surface displacement serves double purposes. One is to minimize the surface displacement, to avoid the potential problem of plasma touching the facing components. Secondly, it appears that the plasma surface displacement is inherently related to the field response, the plasma flow, and even the density pump out behaviour observed in the RMP experiments [24, 30, 31]. Therefore, it not unreasonable to assume that the surface displacement is associated with the mode locking, and hence can be used to design criteria for the purpose of the EFC to avoid the mode locking. In fact, as will be shown in the next section, it seems that certain criterion based on the plasma surface displacement does give a good indication for the optimal EFC in MAST.

We consider several possibilities in designing the criterion C for the EFC optimization, namely the maximal magnitude of the displacement (with respect to the equilibrium surface) along the poloidal circumference, the average magnitude of the displacement, the outboard mid-plane displacement, and the displacement near the X-point. The latter two choices are motivated by the recently observed correlation between the density pump out in MAST and the plasma X-point displacement due to the linear response to the RMP field [24].

4.4. Criterion D: minimization of EF based on SVD

The EFC based on the singular value decomposition (SVD) technique has recently been applied to both DIII-D [13] and ITER [12] plasmas. The basic idea is the following. Suppose a stable plasma response to an imposed external vacuum field is the superposition of the response from all stable eigenmodes of the system, for a given toroidal mode number n. In the discrete level (e.g. in the poloidal Fourier space), the response of all the eigenmodes forms a response matrix. The diagonal elements of the SVD of this response matrix indicates the sensitivity of the plasma response to the corresponding eigenvector. In other words, the strongest response from the plasma corresponds to the largest singular value of the $M \times M$ response matrix, where M is the total number of poloidal harmonics for a given toroidal number n. Therefore, by projecting the EF into the basic system of the SVD eigenvectors, and correcting (i.e. cancelling) the most sensitive component using the EFCC field, we expect to significantly reduce the plasma response to the EF field. We emphasize that the most sensitive SVD eigenvector generally contains all the poloidal Fourier harmonics, i.e. does not correspond to a single Fourier harmonic. This technique has been shown to be rather successful in interpreting the EFC experiments in DIII-D using the internal coils (the I-coils) [13]. It is reasonable to assume that the SVD based correction is more efficient in the presence of a strong amplification (the resonant field amplification (RFA) of the EF by the plasma response.

The SVD approach, employed in [12], assumes an ideal plasma response without plasma flow. In this work, we consider both resistive and ideal plasma response models, as defined in section 3.1, in the SVD based optimization criterion. A numerical example will be given in the next Section, to show how this technique works.

5. Modelling results and comparison with experiments

We have performed extensive modelling of the EFC in MAST, for various plasma configurations. We start by showing the numerical results for a typical case, for the discharge 26128. This is a L-mode discharge at 0.5 T toroidal magnetic field and 600 kA plasma current. The equilibrium is reconstructed at the time of 220 ms. The normalized plasma pressure, β_N, is about 1. The core plasma flow speed is about 1.3% of the Alfvén speed. We apply each of the above described criteria, and compare the results with the empirical data.

5.1. A case study

Figure 7 shows the results according to criterion A, using (a) the vacuum only, and (b) the plasma response field as well. The contour plots of the amplitude of the total (i.e. EF + EFCC) resonant radial field at the $q = 2$ surface show the level of correction while varying the coil currents in two pairs of EFCC. The vacuum criterion predicts the optimal correction currents of $I_1 = -0.5$ kAt and $I_2 = -0.75$ kAt for this discharge, whilst the empirically measured optimum is $I_1 = -0.81$ kAt, $I_2 = -1.91$ kAt. The resistive plasma response model gives a much better prediction, with the optimum $I_1 = -1.10$ kAt, $I_2 = -1.75$ kAt.

It is interesting to point out that, suppose there were no toroidal coupling effect, then the plasma response to the 2/1 component of the EF vacuum field and to the 2/1 component of the vacuum EFCC field should have been identical. Therefore, criterion A should have predicted the same optimal EFCC currents with or without the plasma response. The fact that the optimum with the plasma response agrees better with experiments, than the vacuum criterion, indicates the importance of the toroidal coupling effect.

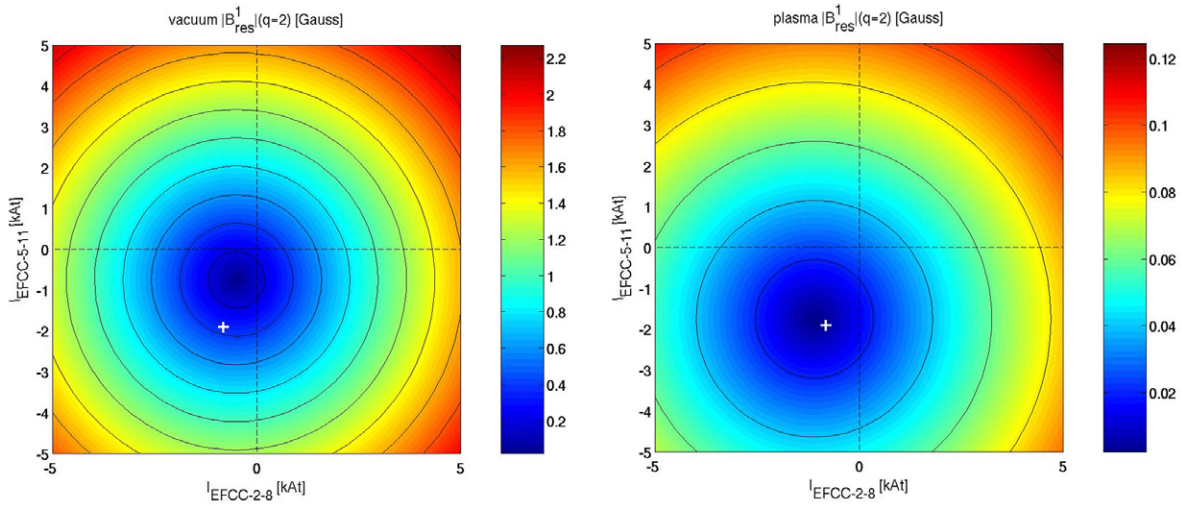

Figure 7. EFC following criterion A: minimize the amplitude of the $m/n = 2/1$ resonant radial field at the $q = 2$ surface, for (a) the vacuum field only and (b) the total response field. The symbol '+' indicates the empirical optimum.

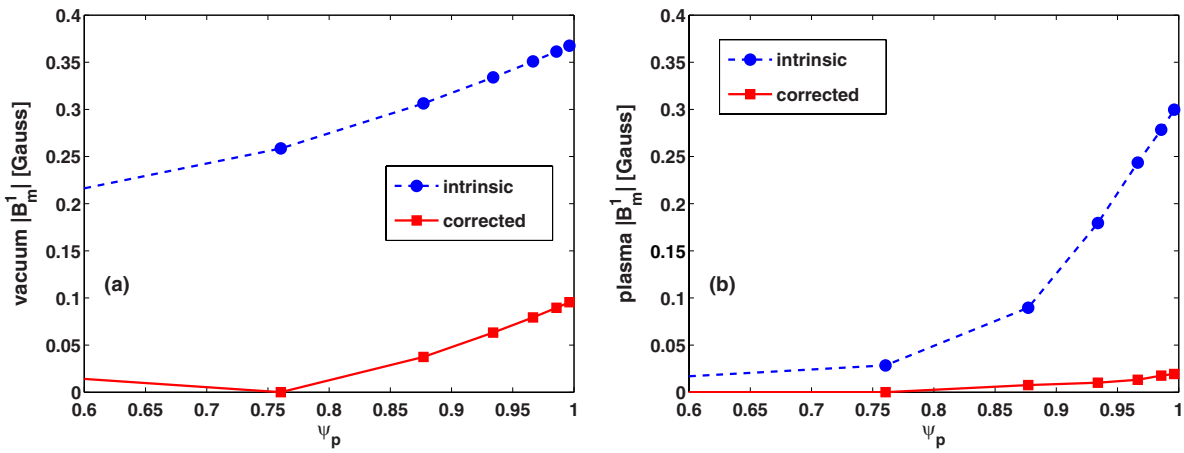

Figure 8. Comparison of the amplitude of the resonant harmonics ($m = 2, 3, 4, 5, 6, 7$) of the radial EF at corresponding rational surfaces before and after the optimal correction according to criterion A, for (a) the vacuum field only and (b) including the plasma response.

Even though criterion A aims only at correcting the 2/1 resonant field, the same (optimal) EFCC currents also give significant correction of the other resonant harmonics, as shown in figure 8. Here, the $m = 2$ harmonic of the EF is fully cancelled by the EFCC field. The other resonant harmonics ($m = 3$–7) are also partially corrected. This is particularly efficient when the plasma response is taken into account.

Next, we consider the EFC using criterion B. Figure 9(a) shows the contour plot of the net EM torque across the plasma volume, as a result of the resistive plasma response to the combined vacuum field from both EF and EFCC. (Note that we only consider the resistive plasma model here, although an ideal plasma response can also generate a finite net $\boldsymbol{j} \times \boldsymbol{b}$ torque [29, 32]. This finite torque comes from the continuum resonances in an ideal plasma, and is often smaller than that from a resistive plasma response.) The predicted optimal correction point, according to this criterion, is $I_1 = -1.15$ kAt, $I_2 = -1.70$ kAt, again reasonably close to the empirical optimum. It is interesting to note that the predicted optimum again reduces significantly the amplitude of all the resonant harmonics, as shown by figure 9(b), although this time the amplitude of the 2/1 harmonic does not exactly vanish.

Figure 10 shows the contour plots of the amplitude of various plasma surface displacement quantities, in the presence of the EF and the varying EFCC currents I_1, I_2. Again the resistive plasma model is assumed. The criteria of minimizing the maximal, the mean, the outboard mid-plane, and the X-point displacement produce the optimal points of $(I_1, I_2) = (-1.15, -1.87)$, $(-1.13, -1.81)$, $(-1.61, -0.23)$, $(-1.15, -1.89)$ kAt, respectively. For this specific discharge, all but the mid-plane displacement criteria predict reasonably well the MAST EFC experiment.

We notice that the contour lines in figures 7, 10(c) and (d) form perfect circles. This can be shown to be always the case if the objective function used in the optimization criterion involves a local linear quantity, such as the EFCC induced resonant field at the $q = 2$ surface, the EFCC induced plasma surface displacement at a given poloidal location, etc. The reason is that these $n = 1$ local quantities always scales linearly with the $n = 1$ component of the EFCC current, $I^{n=1}_{\mathrm{EFCC}}$,

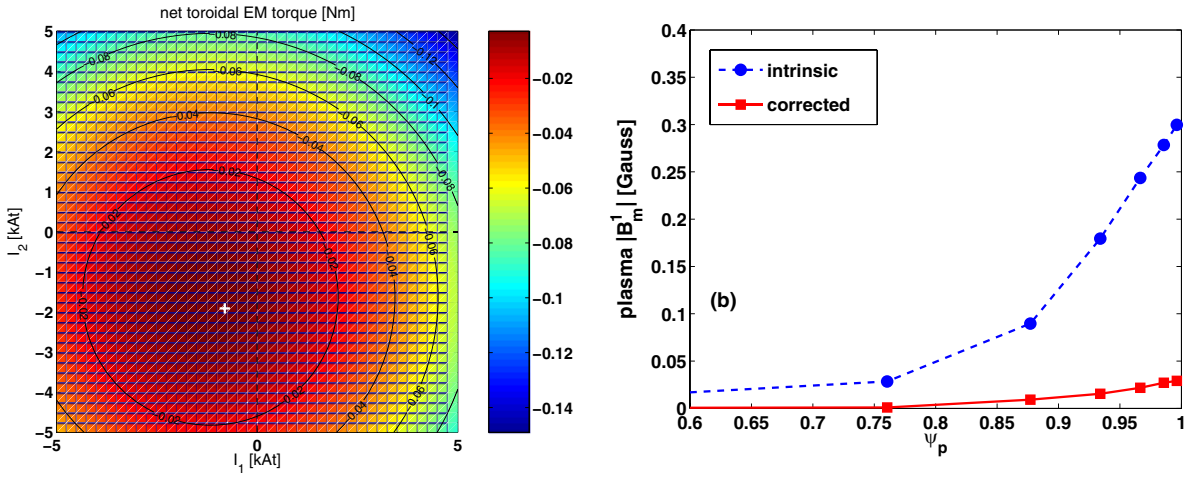

Figure 9. (*a*) EFC following criterion B: minimize the net EM torque acting on the plasma column. The symbol '+' indicates the empirical optimum. (*b*) Comparison of the amplitude of the resonant harmonics ($m = 2, 3, 4, 5, 6, 7$) of the radial EF at corresponding rational surfaces before and after the optimal correction according to criterion B.

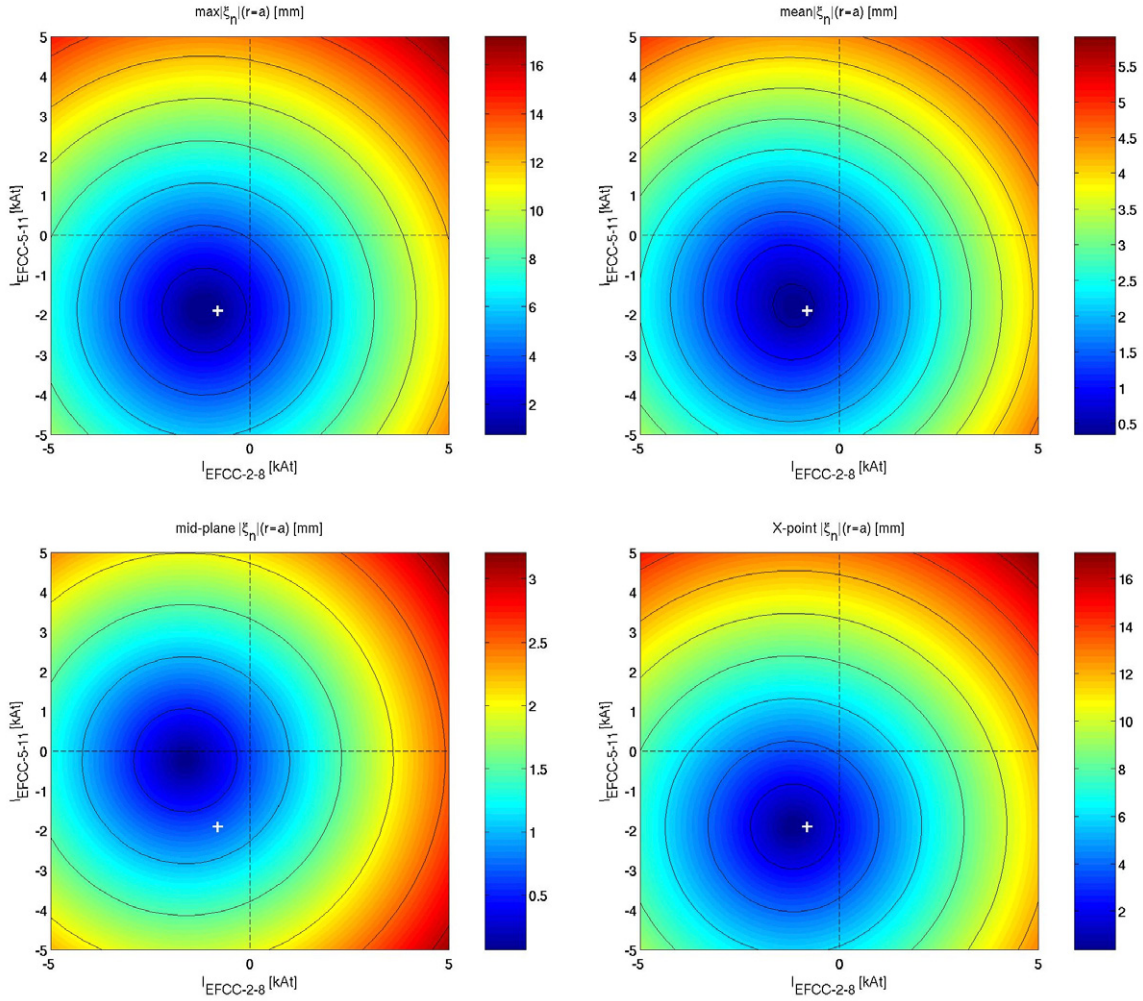

Figure 10. EFC following criterion C: minimize the amplitude of the normal displacement of the plasma surface in terms of (*a*) the maximal displacement along the poloidal angle, (*b*) the surface averaged displacement amplitude, (*c*) the outboard mid-plane displacement and (*d*) the *X*-point displacement. The symbol '+' indicates the empirical optimum.

which in turn, as can be easily shown, scales linearly with the combination of the pair of the coil currents I_1 and I_2 as follows

$$I_{\mathrm{EFCC}}^{n=1} = C_1[(I_1 - I_2) + i(I_1 + I_2)]. \quad (6)$$

Taking an example of the criterion A, where we optimize the resonant field at the $q = 2$ surface. The objective function is defined as $F \equiv |\alpha b_{\mathrm{EFCC}}^{\mathrm{res}} + b_{\mathrm{EF}}^{\mathrm{res}}|$, where the field can be either the vacuum field alone or that including the plasma response.

In either case, we have a linear relation $b^{\rm res}_{\rm EFCC} = C_2 I^{n=1}_{\rm EFCC}$. Therefore,

$$F = |\alpha C_2 I^{n=1}_{\rm EFCC} + b^{\rm res}_{\rm EF}| \quad (7)$$

$$= |\alpha C_2 C_1[(I_1 - I_2) + i(I_1 + I_2)] + b^{\rm res}_{\rm EF}| \quad (8)$$

$$= C_3|(1+i)I_1 - (1-i)I_2 - C_4| \quad (9)$$

$$= C_3|(1+i)(I_1 - I_1^{\rm opt}) - (1-i)(I_2 - I_2^{\rm opt})| \quad (10)$$

$$= \sqrt{2}C_3\left[(I_1 - I_1^{\rm opt})^2 + (I_2 - I_2^{\rm opt})^2\right]^{1/2}, \quad (11)$$

which gives exact circles for the contour lines of the objective function F. Note that $C_3 \equiv |\alpha C_1 C_2|$ in the above derivations, and $C_4 \equiv b^{\rm res}_{\rm EF}/(\alpha C_1 C_2) \equiv (1+i)I_1^{\rm opt} - (1-i)I_2^{\rm opt}$ representing the optimal correction currents.

The criterion based on the net EM torque (figure 9) also results in perfect circles for the contour lines. This is because the net torque is the volume integration of a quantity $\mathrm{conj}(j)b \propto \mathrm{conj}(b)b = |b|^2 \propto |\alpha b_{\rm EFCC} + b_{\rm EF}|^2$. On the other hand, the criterion based on the maximum or the mean value of the surface displacement is not a local linear quantity, and hence the contour curves shown in figures 10(*a*) and (*b*) generally do not have to be exact circles. In fact we found other MAST cases where these contour lines were far from being circles.

Figures 11–14 show the EFC results based on the SVD technique (criterion D) for the MAST discharge 26128. For this, we first compute the plasma response (both ideal and resistive) to the vacuum field generated by each single poloidal harmonic of an external current source. Combining all the responses together allows us to compute the response matrix, that relates the poloidal harmonics of the normal component of any vacuum field to that of the total plasma response field. The singular values of this matrix are sorted in a decreasing order, and plotted in figure 11. (We include 59 poloidal harmonics in the plasma response computations, which defines the dimension of the response matrix, and hence the number of the singular values shown in the figure.) The singular values from the resistive and the ideal response are compared. In both cases, there is a dominant singular value (the first one in the figure), that corresponds to the most sensitive component of the vacuum field, in terms of the plasma response. The dominance is more pronounced for the ideal plasma response.

Figure 12(*a*) compares the radial component of the vacuum (dashed line) EF and the resistive plasma response (solid line) fields at a surface just outside the plasma boundary. The plasma response in this case does not substantially change the vacuum EF, but a finite modification along certain poloidal angles is still observed. By adding an EFCC field in such a way, that the eigenvector corresponding to the first singular value is completely removed from the vacuum EF, we obtain the new (combined) vacuum field and the plasma response in figure 12(*b*). We notice that the overall modification of the vacuum field, by the plasma response, is even less in this case compared to figure 12(*a*), thanks to the removal of the most sensitive component. It is interesting to note that the combined vacuum field (EF + optimal EFCC according to SVD) is slightly larger, in average, than the vacuum EF alone. This is because the SVD technique does not aim at reducing the average vacuum EF.

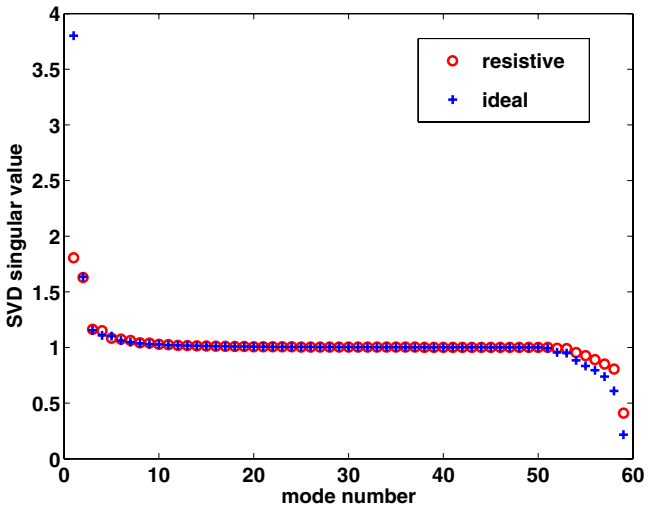

Figure 11. The singular values of the plasma response matrices computed for the $n = 1$ normal field at the vacuum surface $S_{\rm EF}$, assuming a resistive plasma with toroidal flow (o) and an ideal plasma without flow (+).

The effect of the SVD technique is more dramatic for the ideal plasma response, as shown in figure 13. In this case, because the plasma response does bring a significant amplification of the vacuum EF (can also be seen in figure 5(*a*)), removal of the most sensitive component from the vacuum EF significantly reduces the plasma response (figure 13(*b*)), but unfortunately at the expense of increasing the overall combined vacuum field.

We point out a subtle difference in our approach of applying the SVD technique to the ideal plasma response, compared to that adopted by the IPEC code [12]. We apply the SVD technique directly to the MARS-F computed total ideal response field (at surface $S_{\rm EF}$ as shown in figure 13, as well as at the $q = 2$ surface in later results). The results thus can be directly compared with that from the resistive response model. The IPEC approach, on the other hand, further computes an equivalent total plasma response after the ideal run, which corresponds to the field assuming a complete decay of the plasma shielding currents formed by the ideal response.

The optimal EFCC currents, that give the full cancellation of the most sensitive component of the vacuum EF according to the SVD criterion, are plotted in figure 14, and compared to the empirical optimum (point 'E'). We considered both the resistive and ideal plasma response models, and applied the SVD criterion to the radial field located at a surface just outside the plasma (as shown in the above figures 11–13), as well as the radial field located at the $q = 2$ surface. This gives four combinations, shown by points (1)–(4) in figure 14. For the MAST plasma, the SVD criterion does not seem to predict the optimal EFC well, compared to that in DIII-D [13]. This may be due to rather different plasma configurations (the beta value, the aspect ratio, the toroidal flow, possibly the difference in the correction coil geometry, etc.) between MAST and DIII-D. For the ideal response, this should also be associated with the subtle difference mentioned above, on how two codes (MARS-F versus IPEC) treat the ideal response field.

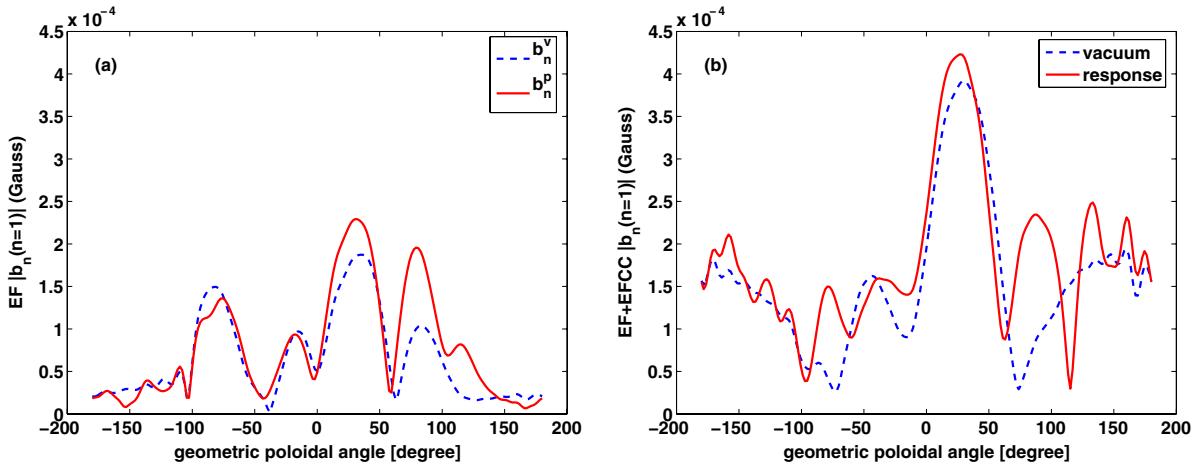

Figure 12. The normal component of the vacuum and the plasma response fields at the surface S_{EF}, for (a) the intrinsic EF alone, and (b) the corrected EF based on the SVD criterion. A resistive plasma with toroidal flow is assumed.

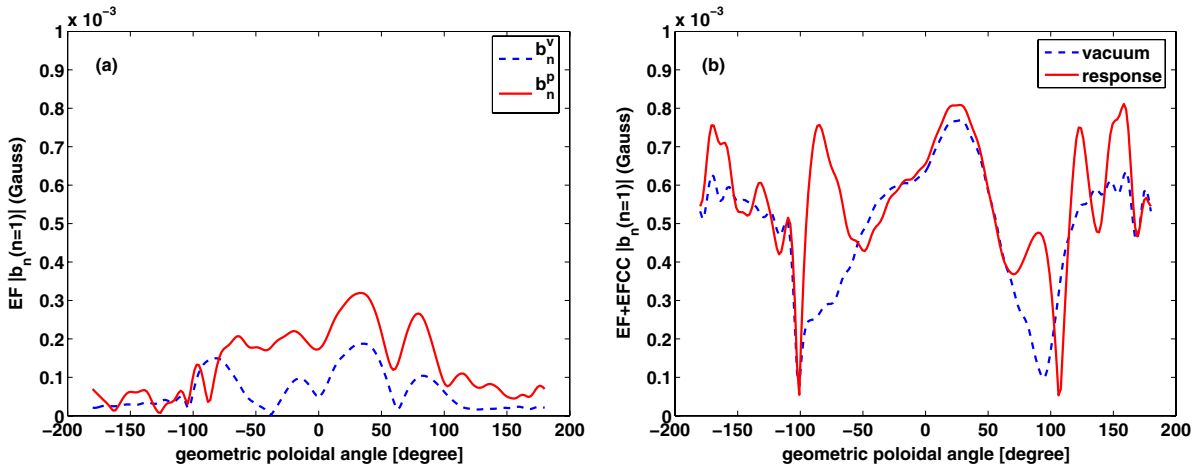

Figure 13. The normal component of the vacuum and the plasma response fields at the surface S_{EF}, for (a) the intrinsic EF alone, and (b) the corrected EF based on the SVD criterion. An ideal static plasma is assumed.

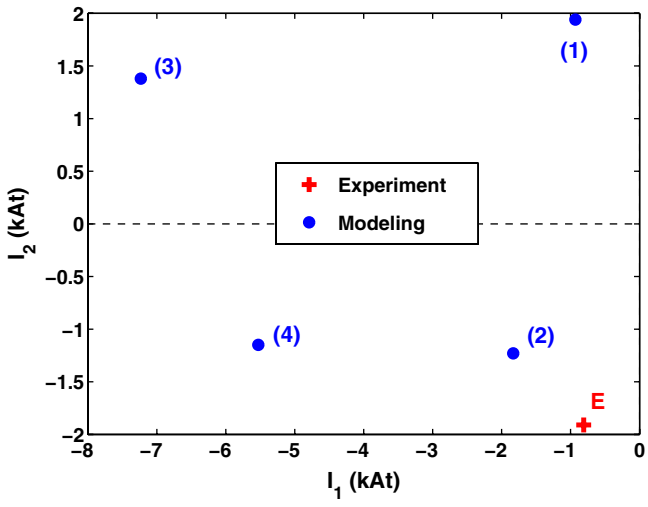

Figure 14. Comparison of the optimal EFCC currents for correcting the $n = 1$ EF in MAST 26128 according to the SVD criterion, based on various response fields: (1)—field just outside plasma surface (S_{EF}) from a resistive plasma model, (2)—field at the $q = 2$ surface from a resistive plasma model, (3)—field just outside plasma surface (S_{EF}) from an ideal plasma model, (4)—field at the $q = 2$ surface from an ideal plasma model, E—the empirical optimal current.

5.2. All cases

We repeated the above study, assuming criteria A–C, for six representative MAST L-mode plasmas, where the EFC experiments had been carried out. These cases cover the plasma line averaged density variation between 1.12×10^{19} and 2.65×10^{19} m^{-3}. The Greenwald limit normalized density varies between 0.31 and 0.48. The ratio of the PF coil currents, P4 to P5, varies between 0.5 and 4. (The P4 and P5 are the major source of the EF in MAST [19].) The results are summarized in the following figures, where each figure corresponds to one criterion. We plot the predicted optimal correction currents along the vertical axis, and the empirical optimum along the horizontal axis. The dashed line in each figure represents perfect agreement between theory and experiments. The pair of the EFCC currents (I_1, I_2) are connected by straight lines.

Figure 15 reports the comparison based on criterion A with (a) vacuum field alone, and (b) resistive plasma response field. The vacuum criterion tends to systematically under-estimate the optimal correction currents. Including the plasma response generally improves the agreement between theory and experiments, but sometimes leads to the over-estimation of the correction currents, in particular for I_2. This nevertheless

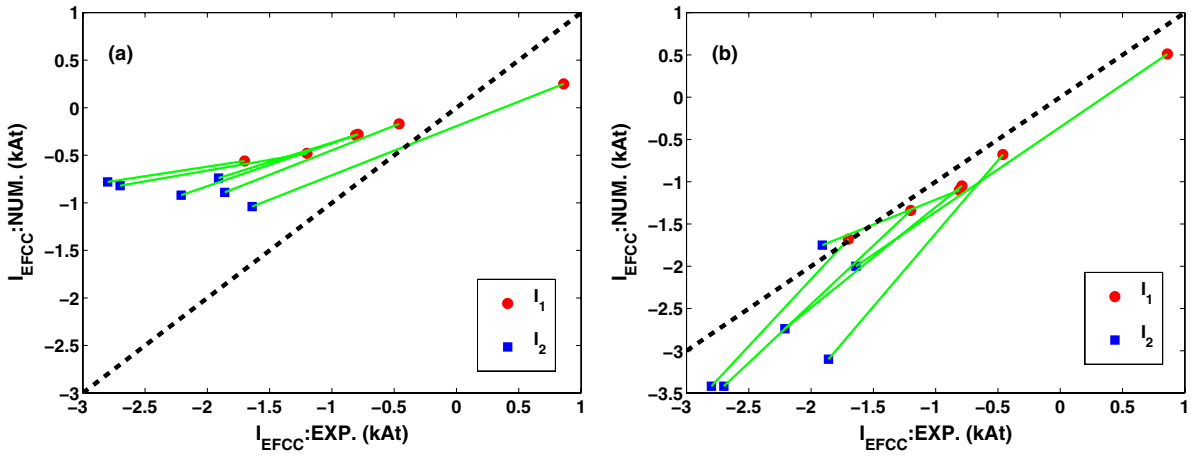

Figure 15. The computed optimal EFCC currents versus the empirical values, for correcting the $n = 1$ EF in various MAST plasmas, using the optimization criterion A for (a) the vacuum field only, and (b) the total resistive response field.

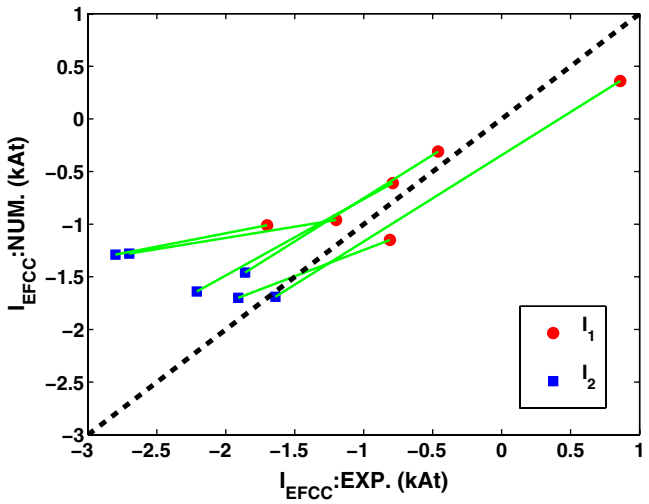

Figure 16. The computed optimal EFCC currents versus the empirical values, for correcting the $n = 1$ EF in various MAST plasmas, using the optimization criterion B for the total resistive response field.

shows the importance of considering the plasma response for the EFC study.

The agreement is somewhat worse, by using criterion B based on minimizing the net EM torque (figure 16). The worst case, from the discharge 26467, has the lowest P4/P5 ratio, and is also the worst case with criterion A. From the experimental side, this case also has the largest radius of the circle in the (I_1, I_2) plane, formed by the four marginal locking/unlocking points. Therefore, the experimental uncertainty for the empirical optimal point (the centre of the circle) is also the largest. The overall agreement, according to criterion B, is better than the vacuum field based criterion A.

The next figure (figure 17) summarizes the comparison based on criterion C. Generally we find that the criteria using certain global quantities of the displacement, such as the peak value along the poloidal angle of the plasma surface, or the mean value, gives a better agreement with experiments. The local displacement based criteria (either the outboard midplane or the X-point displacement) yield more scattering of the results and less agreement with experiments. Overall, the best agreement, among the displacement based criteria, seems to be achieved by using the surface averaged displacement amplitude as the minimization criterion for the EFC in MAST.

The results shown above are also summarized in tables 1–7. Since in our study, what really matters is the $n = 1$ component of the current produced by EFCC, we compare a complex quantity $I \equiv (I_1 - I_2) + (I_1 + I_2) * i$ in these tables following equation (6), between the empirical and the numerical values. We also show the average errors in both amplitude and phase in each table (i.e. for each criterion). However, these average values should be taken with care, because the selected discharges are generally not uniformally distributed among the whole database. Nevertheless, these tables confirm the observations from figures 15–17. In particular, we notice that the plasma response based criterion A, the EM torque based criterion B, as well as the mean displacement and the X-point displacement based crietria C, all perform with similar accuracy. These criteria provide reasonably accurate prediction for the toroidal phase of the optimal correcting field, except the discharge 26271, for which all the criteria result in a large phase error. For this discharge, the empirically determined optimal phase also significantly differs from that of other discharges. Further investigation is needed to pinpoint the reason.

As discussed in the previous subsection, the global displacement criterion (either the peak or the average) do not generally produce circular contour lines in the (I_1, I_2) plane. On the other hand, the experimentally measured marginal EFCC currents (locked mode limit) in MAST often tend to form a reasonable circle [19]. Nevertheless, the optimal points produced by the global displacement criteria seem to agree well with the empirical optima, and therefore can still be useful for predicting the EFC currents for experiments.

6. Conclusion and discussion

We have numerically investigated the correction of the error field in MAST plasmas, by optimizing the EFCC currents. The

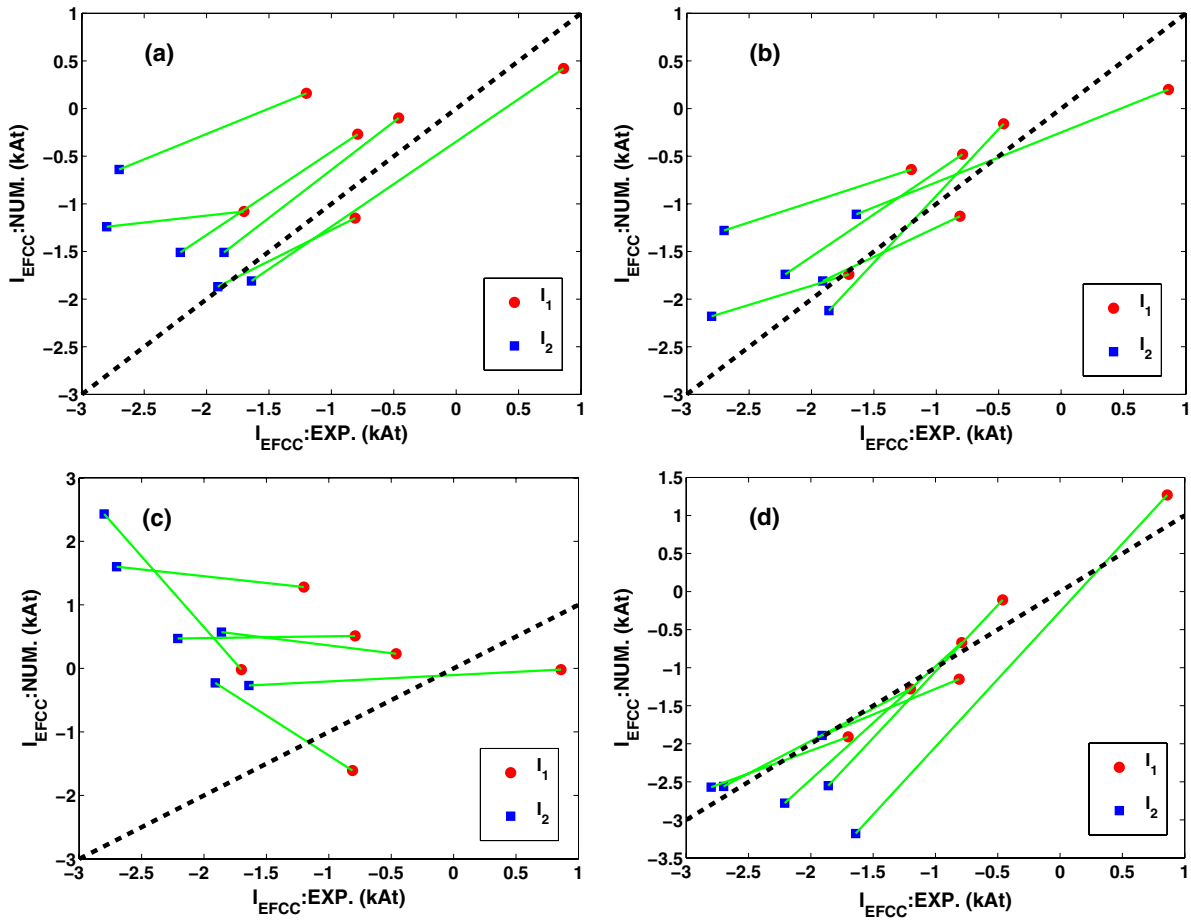

Figure 17. The computed optimal EFCC currents versus the empirical values, for correcting the $n = 1$ EF in various MAST plasmas, using the optimization criterion C for (a) the maximal plasma surface displacement, (b) the mean value of the surface displacement, (c) the outboard mid-plane surface displacement, and (d) the surface displacement near the X-point.

Table 1. Comparison between empirical and numerical optima for the $n = 1$ EFCC current amplitude and phase, using the vacuum field based optimization criterion A.

Shot#	$\|I_{EXP}\|$ (kAt)	$\|I_{NUM}\|$ (kAt)	$\|\Delta I\|$ (kAt)	$\|\Delta I\|/\|I_{EXP}\|$	$\angle I_{EXP}$ (deg)	$\angle I_{NUM}$ (deg)	$\|\Delta\angle I\|$ (deg)
26 271	2.61	1.51	1.21	46.2	−17.3	−31.4	14.1
26 051	3.31	1.36	1.96	59.1	−64.6	−61.9	2.74
10 738	2.70	1.28	1.43	52.8	−58.8	−55.8	3.07
26 467	4.63	1.35	3.28	70.8	−76.2	−80.6	4.41
26 128	2.93	1.12	1.81	61.7	−67.9	−66.4	1.58
28 995	4.17	1.34	2.84	68.1	−68.9	−75.3	6.38
Average	—	—	—	59.8	—	—	5.39

Table 2. Comparison between empirical and numerical optima for the $n = 1$ EFCC current amplitude and phase, using the total resistive response field based optimization criterion A.

Shot#	$\|I_{EXP}\|$ (kAt)	$\|I_{NUM}\|$ (kAt)	$\|\Delta I\|$ (kAt)	$\|\Delta I\|/\|I_{EXP}\|$	$\angle I_{EXP}$ (deg)	$\angle I_{NUM}$ (deg)	$\|\Delta\angle I\|$ (deg)
26 271	2.61	2.91	0.71	27.1	−17.3	−30.6	13.3
26 051	3.31	4.14	0.83	25.1	−64.6	−65.9	1.29
10 738	2.70	4.48	1.78	65.7	−58.8	−57.3	1.51
26 467	4.63	5.38	0.87	18.9	−76.2	−71.1	5.10
26 128	2.93	2.92	0.46	15.9	−67.9	−77.1	9.17
28 995	4.17	5.19	1.03	24.8	−68.9	−66.3	2.56
Average	—	—	—	29.6	—	—	5.50

study is mainly based on the linear plasma response, assuming both resistive and ideal plasma models as defined in this work. Various criteria have been considered for achieving the best correction of the EF. The predicted optimal correction currents are compared with empirical data, in order to find the best criterion (at least for MAST plasmas).

We find that it is important to include the plasma response, in order to correctly predict the EFC experiments in MAST.

Table 3. Comparison between empirical and numerical optima for the $n = 1$ EFCC current amplitude and phase, using the $\boldsymbol{j} \times \boldsymbol{b}$ torque based optimization criterion B.

Shot#	$\lvert I_{EXP}\rvert$ (kAt)	$\lvert I_{NUM}\rvert$ (kAt)	$\lvert\Delta I\rvert$ (kAt)	$\lvert\Delta I\rvert/\lvert I_{EXP}\rvert$	$\angle I_{EXP}$ (deg)	$\angle I_{NUM}$ (deg)	$\lvert\Delta\angle I\rvert$ (deg)
26 271	2.61	2.44	0.71	27.1	−17.3	−32.9	15.6
26 051	3.31	2.47	0.84	25.4	−64.6	−65.4	0.73
10 738	2.70	2.11	0.60	22.2	−58.8	−56.9	1.90
26 467	4.63	2.31	2.34	50.6	−76.2	−83.0	6.79
26 128	2.93	2.90	0.56	19.2	−67.9	−79.0	11.0
28 995	4.17	2.26	2.03	48.7	−68.9	−81.8	12.9
Average	—	—	—	32.2	—	—	8.18

Table 4. Comparison between empirical and numerical optima for the $n = 1$ EFCC current amplitude and phase, using the maximal plasma surface displacement based optimization criterion C.

Shot#	$\lvert I_{EXP}\rvert$ (kAt)	$\lvert I_{NUM}\rvert$ (kAt)	$\lvert\Delta I\rvert$ (kAt)	$\lvert\Delta I\rvert/\lvert I_{EXP}\rvert$	$\angle I_{EXP}$ (deg)	$\angle I_{NUM}$ (deg)	$\lvert\Delta\angle I\rvert$ (deg)
26 271	2.61	2.62	0.66	25.4	−17.3	−31.9	14.6
26 051	3.31	2.16	1.23	37.1	−64.6	−55.1	9.53
10 738	2.70	2.14	0.71	26.2	−58.8	−48.7	10.1
26 467	4.63	2.32	2.37	51.2	−76.2	−86.0	9.79
26 128	2.93	3.10	0.48	16.5	−67.9	−76.5	8.60
28 995	4.17	0.93	3.49	83.5	−68.9	−30.9	37.9
Average	—	—	—	40.0	—	—	15.1

Table 5. Comparison between empirical and numerical optima for the $n = 1$ EFCC current amplitude and phase, using the mean value of the plasma surface displacement based optimization criterion C.

Shot#	$\lvert I_{EXP}\rvert$ (kAt)	$\lvert I_{NUM}\rvert$ (kAt)	$\lvert\Delta I\rvert$ (kAt)	$\lvert\Delta I\rvert/\lvert I_{EXP}\rvert$	$\angle I_{EXP}$ (deg)	$\angle I_{NUM}$ (deg)	$\lvert\Delta\angle I\rvert$ (deg)
26 271	2.61	1.59	1.19	45.7	−17.3	−34.7	17.4
26 051	3.31	2.55	0.79	23.9	−64.6	−60.4	4.24
10 738	2.70	3.00	0.56	20.7	−58.8	−49.3	9.57
26 467	4.63	3.94	0.87	18.9	−76.2	−83.5	7.33
26 128	2.93	3.01	0.47	16.1	−67.9	−76.9	8.99
28 995	4.17	2.02	2.15	51.6	−68.9	−71.5	2.60
Average	—	—	—	29.5	—	—	8.36

Table 6. Comparison between empirical and numerical optima for the $n = 1$ EFCC current amplitude and phase, using the outboard mid-plane plasma surface displacement based optimization criterion C.

Shot#	$\lvert I_{EXP}\rvert$ (kAt)	$\lvert I_{NUM}\rvert$ (kAt)	$\lvert\Delta I\rvert$ (kAt)	$\lvert\Delta I\rvert/\lvert I_{EXP}\rvert$	$\angle I_{EXP}$ (deg)	$\angle I_{NUM}$ (deg)	$\lvert\Delta\angle I\rvert$ (deg)
26 271	2.61	0.38	2.30	87.9	−17.3	−49.2	31.9
26 051	3.31	0.98	4.21	126.0	−64.6	87.6	152.0
10 738	2.70	0.86	3.57	131.0	−58.8	113.0	171.0
26 467	4.63	3.43	7.76	167.0	−76.2	135.0	211.0
26 128	2.93	2.30	2.63	89.6	−67.9	−126.0	58.8
28 995	4.17	2.89	7.02	168.0	−68.9	96.3	165.
Average	—	—	—	128.0	—	—	132.

A similar conclusion has been achieved in the modelling of the EFC for DIII-D L-mode plasmas [13]. Based on a full cancellation of the 2/1 resonant field at the $q = 2$ surface, the resistive plasma response model predicts the optimal correction currents which are in better agreement with experiments, than the vacuum model. This fact itself is a manifestation of strong coupling of the Fourier harmonics in MAST plasmas, introduced by the toroidicity and the plasma shaping.

Comparing the optimal correction currents between theory and experiments for various plasma and EF configurations in MAST, we find that the following two correction criteria work the best for MAST. One corresponds to the full cancellation of $2/1$ resonant harmonic at the $q = 2$ rational surface, including the plasma response; the other is to minimize the net electromagnetic torque across the plasma volume. The displacement criteria do not generally produce circular contour lines in the polar map plane (I_1, I_2), and do not generally produce satisfactory predictions for the optimal correction currents. It remains the future work to apply these criteria to other devices such as DIII-D, where extensive experimental data are available.

It is interesting to note that the torque criteria B involves global characteristics of the plasma response, associated with neither a single surface of the plasma nor a single mode response from the plasma. The results of the proxy EF experiments in DIII-D also seem to suggest the need for a global correction criterion [33]. Whilst the net EM torque

Table 7. Comparison between empirical and numerical optima for the $n = 1$ EFCC current amplitude and phase, using the near X-point plasma surface displacement based optimization criterion C.

Shot#	$\|I_{EXP}\|$ (kAt)	$\|I_{NUM}\|$ (kAt)	$\|\Delta I\|$ (kAt)	$\|\Delta I\|/\|I_{EXP}\|$	$\angle I_{EXP}$ (deg)	$\angle I_{NUM}$ (deg)	$\|\Delta\angle I\|$ (deg)
26 271	2.61	4.84	2.25	86.0	−17.3	−23.2	5.90
26 051	3.31	4.04	0.82	24.8	−64.6	−58.5	6.12
10 738	2.70	3.60	1.09	40.3	−58.8	−47.4	11.4
26 467	4.63	4.52	0.44	9.50	−76.2	−81.6	5.35
26 128	2.93	3.12	0.48	16.4	−67.9	−76.3	8.33
28 995	4.17	4.04	0.22	5.45	−68.9	−71.5	2.60
Average	—	—	—	30.4	—	—	6.62

criterion is directly associated with the flow damping for the mode locking, the displacement criteria can also be related to the generic requirement of minimizing the EF caused 3D distortion of the plasma surface. The latter can be a critical issue if the tokamak is operated with a very narrow gap between the plasma surface and the first material wall.

We also find that the SVD based optimization criterion does not produce satisfactory comparison with experiments for the EFC in MAST. This is the case for both resistive and ideal plasma response models adopted in this study. The SVD approach has been reported working reasonably well for DIII-D plasmas [13]. We attribute this discrepancy to the differences in the plasma and coil configurations between the two devices, as well as to the different treatment of the ideal plasma response when the SVD technique is applied. Further work, in particular the cross-machine comparison of the EFC modelling, needs to be carried out, before reaching a confident prediction for the EFC in ITER.

In this work, we have not considered the possibility of combining various optimization criteria, to form a more generic one. This may be necessary for cases where the polar map from experiments shows a shape which is far from a circle. This is so far not the case for MAST plasmas. We have not yet modelled the EFC using the RMP coils in MAST, although a limited number of such experiments have been carried out.

Appendix A. Derivation of inductance matrix between ESC and normal EF in a generic toroidal geometry

A generic toroidal geometry is described by a curve-linear coordinate system (s, χ, ϕ), with s labelling the minor radius, χ being a generalized poloidal angle, and ϕ the geometric toroidal angle of the torus. We choose a contravariant representation for the coil current $\boldsymbol{J}$, and the magnetic field $\boldsymbol{B}$ produced by $\boldsymbol{J}$ in free space,

$$\boldsymbol{B} = B^1\nabla\chi\times\nabla\phi + B^2\nabla\phi\times\nabla s + B^3\nabla s\times\nabla\chi, \quad (12)$$

$$\boldsymbol{J} = J^1\nabla\chi\times\nabla\phi + J^2\nabla\phi\times\nabla s + J^3\nabla s\times\nabla\chi, \quad (13)$$

and decompose all the field components in Fourier space along the poloidal and toroidal angles, e.g.,

$$B^1(s,\chi,\phi) = \sum_m B^1(s)\exp(\mathrm{i}m\chi - \mathrm{i}n\phi), \quad (14)$$

$$J^2(s,\chi,\phi) = \sum_m J^2(s)\exp(\mathrm{i}m\chi - \mathrm{i}n\phi). \quad (15)$$

Note that in the above expressions, we have assumed a single toroidal harmonic $n \neq 0$ for the current and the field. We further assume a surface current (i.e. ESC) $\boldsymbol{J} = (0, J^2, J^3)$ located at the minor radius $s = s_1$. The divergence-free condition for the surface current, $\nabla\cdot\boldsymbol{J} = 0$, or equivalently $\partial J^2/\partial\chi + \partial J^3/\partial\phi = 0$, uniquely defines the toroidal component J^3, by a given poloidal component J^2.

We wish to calculate the mutual inductance matrix $\boldsymbol{A} = \{A_{mk}\}$, that couples the poloidal Fourier harmonics of the radial field B^1, at a surface $s = s_2$, with that of the poloidal component J^2 of the surface current $\boldsymbol{J}$ at $s = s_1$

$$B^1_m(s_2) = \sum_k A_{mk}J^2_k(s_1). \quad (16)$$

The calculation is based on the Biot–Savart law

$$\boldsymbol{B}(\vec{\mathbb{R}}_2) = \frac{\mu_0}{4\pi}\int_v \frac{\boldsymbol{J}\times\vec{\mathbb{R}}}{\mathbb{R}^3}\mathrm{d}v, \quad (17)$$

where $\boldsymbol{J}(\vec{\mathbb{R}}_1) = \boldsymbol{J}_s\delta(s - s_1)$ is the (volumetric) current density, and $\vec{\mathbb{R}} \equiv \vec{\mathbb{R}}_2 - \vec{\mathbb{R}}_1$. We have $\vec{\mathbb{R}}_j = (s_j, \chi_j, \phi_j) = (R_j, \phi_j, Z_j)$, $j = 1, 2$, where (R, ϕ, Z) is the conventional cylindrical coordinates.

It follows that

$$\begin{aligned} B^1 &= R_2\frac{\partial Z_2}{\partial\chi}B_R - R_2\frac{\partial R_2}{\partial\chi}B_Z,\\ B_R &= \frac{\mu_0}{4\pi}\int_v \frac{\boldsymbol{J}\times\vec{\mathbb{R}}\cdot\nabla R_2}{\mathbb{R}^3}\mathrm{d}v,\\ B_Z &= \frac{\mu_0}{4\pi}\int_v \frac{\boldsymbol{J}\times\vec{\mathbb{R}}\cdot\nabla Z_2}{\mathbb{R}^3}\mathrm{d}v, \end{aligned} \quad (18)$$

and

$$\boldsymbol{J}\times\vec{\mathbb{R}}\cdot\nabla R_2 = R_1J_Z\sin\tilde{\phi} + (Z_2 - Z_1)(J_R\sin\tilde{\phi} + J_\phi\cos\tilde{\phi}), \quad (19)$$

$$\boldsymbol{J}\times\vec{\mathbb{R}}\cdot\nabla Z_2 = (R_1 - R_2\cos\tilde{\phi})J_\phi - R_2J_R\sin\tilde{\phi}, \quad (20)$$

where $\tilde{\phi} \equiv \phi_1 - \phi_2$.

We now insert the poloidal Fourier expansions for both B^1 and J^2, equations (14) and (15), into equation (18), and also use the equality $J^3_k = -kJ^2_k/n$ obtained from the divergence-free condition. After straightforward algebraic manipulations,

we derive the final expression for the elements of the coupling matrix $\boldsymbol{A}$ as defined in equation (16)

$$A_{mk} = \frac{\mu_0 k}{8\pi^2 n}\oint \frac{R_1 R_2 \cos(n\tilde{\phi})}{\mathbb{R}^3}\left[(R_1 - R_2\cos\tilde{\phi})\frac{\partial R_2}{\partial \chi} - (Z_2 - Z_1)\cos\tilde{\phi}\frac{\partial Z_2}{\partial \chi}\right] e^{ik\chi_1 - im\chi_2} d\chi_1 d\chi_2 d\tilde{\phi}$$
$$+\frac{i\mu_0}{8\pi^2}\oint \frac{\sin\tilde{\phi}\sin(n\tilde{\phi})}{\mathbb{R}^3} \times \left[R_1 R_2 \frac{Z_1}{\partial\chi}\frac{\partial Z_2}{\partial\chi} + R_2(Z_2 - Z_1)\frac{\partial R_1}{\partial\chi}\frac{\partial Z_2}{\partial\chi} + R_2^2\frac{\partial R_1}{\partial\chi}\frac{\partial R_2}{\partial\chi}\right] \times e^{ik\chi_1 - im\chi_2} d\chi_1 d\chi_2 d\tilde{\phi},$$

where $\mathbb{R}^2 = R_1^2 + R_2^2 - 2R_1R_2\cos\tilde{\phi} + (Z_2 - Z_1)^2$. Note the integrands in the above integrals are always regular if we assume $s_1 \neq s_2$.

Appendix B. On the plasma screening

We shall illustrate, in general toroidal geometry, the difference between the single fluid and the two-fluid theory in the linear screening physics by the plasma flow, assuming a small perturbation is caused by a static, external magnetic field source. Consider a two-fluid model, in which the momentum equation associated with electrons is written as [34]

$$m_e n_e \frac{d\boldsymbol{V}_e}{dt} = -en_e(\boldsymbol{E} + \boldsymbol{V}_e \times \boldsymbol{B}) - \nabla P_e - \nabla\cdot\pi_e + en_e\left(\frac{\boldsymbol{j}_\parallel}{\sigma_\parallel} + \frac{\boldsymbol{j}_\perp}{\sigma_\perp}\right) - \left(0.71 n_e \nabla_\parallel T_e + \frac{3n_e}{2\omega_{ce}\tau_e B}\boldsymbol{B}\times\nabla_\perp T_e\right), \quad (21)$$

where the terms in the second last brackets correspond to frictional forces, and the terms in the last brackets correspond to thermal forces. In particular, it can be shown that the last thermal force term, associated with the electron diamagnetic flow (due to the temperature gradient), can be combined with the perpendicular current yielding a term $(\boldsymbol{j}_\perp + 1.5en_e\boldsymbol{V}_{*T_e})/\sigma_\perp$ which is perpendicular to the magnetic field $\boldsymbol{B}$. Now we perform three steps. First, we neglect the electron inertia together with the stress tensor term $\nabla\cdot\pi_e$ (or assuming certain form of gyroviscous cancellation under steady state condition). For simplicity, we can also neglect the the thermal forces, and assume $\sigma_\parallel = \sigma_\perp$. Secondly, we perform linearization of the above momentum equation (now effectively the Ohm's law for electrons) with respect to small perturbations. Third, we take the parallel component, with respect to the equilibrium field $\boldsymbol{B}_0$, of the perturbed Ohm's law. Note that all the gradient terms, such as $\nabla\tilde{p}_e$ or $\tilde{\boldsymbol{E}} = -\nabla\tilde{\phi}$, when dotted with $\boldsymbol{B}_0$, vanishes at rational surfaces for the perturbation. Therefore, the above procedure will result in an equation with only two terms left, at rational surfaces

$$-en_e^0\boldsymbol{B}_0\times\boldsymbol{V}_e^0\cdot\delta\boldsymbol{B} + \frac{en_e^0}{\sigma_\parallel}\boldsymbol{B}_0\cdot\delta\boldsymbol{j}_\parallel = 0. \quad (22)$$

This gives the solution for the perturbed parallel currents $\delta j_\parallel = \sigma_\parallel \boldsymbol{b}_0\times\boldsymbol{V}_e^0\cdot\delta\boldsymbol{B}$, where $\boldsymbol{b}_0 \equiv \boldsymbol{B}_0/|\boldsymbol{B}_0|$. These parallel currents, generated at rational surfaces due to the (linear) plasma response to external field perturbations, are responsible for the plasma screening effect. It is clear that the screening vanishes when the equilibrium perpendicular electron flow, $\boldsymbol{V}_{e\perp}^0$ happens to vanish at the corresponding rational surface.

On the other hand, the single fluid Ohm's law reads

$$\boldsymbol{E} + \boldsymbol{V}\times\boldsymbol{B} = \frac{\boldsymbol{j}}{\sigma}, \quad (23)$$

where the fluid velocity $\boldsymbol{V}$ is essentially the ion velocity $\boldsymbol{V}_i$. Performing the above mentioned two last steps in a similar way, we find that the perturbed parallel currents at rational surfaces satisfy $\delta j_\parallel = \sigma\boldsymbol{b}_0\times\boldsymbol{V}_i^0\cdot\delta\boldsymbol{B}$. In other words, according to the single fluid theory, the screening due to the plasma response disappears, if the equilibrium perpendicular flow of ions happens to vanish at rational surfaces.

The above discussion shows that the screening physics is indeed different with different fluid models (the essential difference in fact comes from the neglect of the Hall term in the standard MHD approximation). On the other hand, both single and two-fluid models can predict the flow screening. As a final remark, we point out that the above derivations hold only if no continuum resonance induced splitting effect [29] occurs. If the latter does occur, the perturbed parallel current appears off the rational surface, where the $\boldsymbol{B}_0\cdot\nabla$ operator does not vanish anymore.

Acknowledgments

This work was funded by the RCUK Energy Programme under grant EP/I501045 and the European Communities under the contract of Association between EURATOM and CCFE. To obtain further information on the data and models underlying this paper please contact PublicationsManager@ccfe.ac.uk. The views and opinions expressed herein do not necessarily reflect those of the European Commission.

References

[1] Scoville J T *et al* 1991 *Nucl. Fusion* **31** 875
[2] Buttery R J *et al* 1999 *Nucl. Fusion* **39** 1827
[3] Buttery R J *et al* 2000 *Nucl. Fusion* **40** 807
[4] Wolfe S M *et al* 2005 *Phys. Plasmas* **12** 056110
[5] Howell D F *et al* 2007 *Nucl. Fusion* **47** 1336
[6] Menard J E *et al* 2010 *Nucl. Fusion* **50** 045008
[7] Buttery R J *et al* 2011 *Nucl. Fusion* **51** 073016
[8] Okabayashi M *et al* 2009 *Nucl. Fusion* **49** 125003
[9] Reimerdes H *et al* 2009 *Nucl. Fusion* **49** 115001
[10] In Y *et al* 2010 *Plasma Phys. Control. Fusion* **52** 104004
[11] Drake J R *et al* 2005 *Nucl. Fusion* **45** 557
[12] Park J-K *et al* 2008 *Nucl. Fusion* **48** 045006
[13] Park J-K *et al* 2011 *Nucl. Fusion* **51** 023003
[14] Fitzpatrick R *et al* 1991 *Phys. Fluids* B **3** 644
[15] Fitzpatrick R *et al* 1993 *Nucl. Fusion* **33** 1049
[16] Liu Y Q *et al* 2009 *Plasma Phys. Control. Fusion* **51** 115008
[17] Liu Y Q *et al* 2000 *Phys. Plasmas* **7** 3681
[18] Nardon E *et al* 2007 *J. Nucl. Mater.* **363–365** 1071
[19] Kirk A, Liu Y, Martin R, Howell D, Nardon E and The MAST Team 2014 *Plasma Phys. Control. Fusion* **56** 104003
[20] Liu Y Q *et al* 2010 *Phys. Plasmas* **17** 122502
[21] Ferraro N M *et al* 2012 *Phys. Plasmas* **19** 056105
[22] Lanctot M *et al* 2010 *Phys. Plasmas* **17** 030701

[23] Liu Y Q *et al* 2012 *Plasma Phys. Control. Fusion* **54** 124013
[24] Liu Y Q *et al* 2011 *Nucl. Fusion* **51** 083002
[25] Liu Y Q *et al* 2009 *Plasma Phys. Control. Fusion* **51** 115005
[26] Shaing K C *et al* 2010 *Nucl. Fusion* **50** 025022
[27] Park J-K *et al* 2007 *Phys. Rev. Lett.* **99** 195003
[28] Rozhansky V *et al* 2010 *Nucl. Fusion* **50** 034005
[29] Liu Y Q *et al* 2012 *Phys. Plasmas* **19** 102507
[30] Kirk A *et al* 2010 *Nucl. Fusion* **50** 034008
[31] Nardon E *et al* 2009 *Plasma Phys. Control. Fusion* **51** 124010
[32] Taylor J B 2003 *Phys. Rev. Lett.* **91** 115002
[33] Buttery R J *et al* 2012 *Phys. Plasmas* **19** 056111
[34] Braginskii S I 1965 *Rev. Plasma Phys.* **1** 205